Journal of The Electrochemical Society, **153** (1) G98-G104 (2006)
0013-4651/2005/153(1)/G98/7/$20.00 © The Electrochemical Society, Inc.

Comparative Study of Ni–P–Diamond and Ni–P–CNT Nanocomposite Films

Tzu-Yuan Chao, Guang-Ren Shen, and Y. T. Cheng[z]

Microsystems Integration Laboratory, Department of Electronics Engineering, National Chiao Tung University, Hsinchu 300, Taiwan

Ni–P–diamond and Ni–P carbon nanotube (CNT) nanocomposite films have been synthesized and compared in this paper. Because diamond has different shapes and sizes than CNTs, the nanocomposite films exhibit distinct characteristics. Nanoindentation measurements show that the Young's modulus and hardness of the Ni–P–CNT nanocomposite film electroplated in a bath with 0.028 g/L CNTs increase to 665.9 ± 29.5 GPa and 28.9 ± 4.22 GPa, respectively, which is about four times larger than that of pure nickel. On the contrary, the modulus and hardness of the Ni–P–diamond nanocomposite films decrease with the incorporation of the nanodiamond powders due to the formation of voids and cracks, even though both diamond and CNTs have similar Young's modulus and hardness. For the Ni–P–diamond film plated in the bath with 2.0 g/L nanodiamonds, the values are reduced to 110.5 ± 4.3 and 2.3 ± 0.1 GPa. Nevertheless, the electrothermal actuators made of both Ni–P–CNT and Ni-P-diamond composites can provide four times the maximum elongation, larger than that made of pure nickel. With the same displacement, the input power of the nanocomposite actuators is much less than that of the pure Ni one. This study reveals potential applications for nano/microelectromechanical systems fabrication using both Ni–P–diamond and Ni–P–CNT nanocomposites due to their distinctive physical properties and compatibility with contemporary complementary metal oxide semiconductor manufacturing processes.
 [DOI: 10.1149/1.2133324]

Manuscript submitted June 23, 2005; revised manuscript received September 12, 2005.
Available electronically December 12, 2005.

Previously, we proposed a complementary metal oxide semiconductor (CMOS) compatible process for robust microelectromechanical systems (MEMS) fabrication using selective electroless nanocomposite deposition techniques.[1,2] Via the incorporation of a secondary phase into the Ni matrix, a variety of material properties, such as the coefficient of thermal expansion (CTE), hardness, Young's modulus, and electrical conductivity, can be modified and enhanced. Meanwhile, it has been found that the electrothermal actuators made of the nanocomposite materials reveal excellent performance in terms of mechanical reliability and power efficiency, which makes the composite materials fascinating for low-power nano/microelectromechanical systems (N/MEMS) device applications. Inasmuch as diamond has comparable Young's modulus and hardness to carbon nanotubes (CNTs) and its granular structure is different from the fibrous one of CNTs, the strengthening effects of nickel–phosphorus–diamond powder (Ni–P–diamond) nanocomposite film on device performance could be interesting, as well as that of nickel–phosphorus–carbon nanotube (Ni–P–CNT) nanocomposite film. In addition, due to the shape difference, the nanodiamond powders do not require complicated chemical treatment to prevent self-curl phenomenon and agglomeration in the preparation of Ni–P–diamond colloidal plating solution. That would provide a simpler process for device fabrication. Thus, in this paper, the synthesis of Ni–P–diamond for N/MEMS fabrication is presented and compared with that of Ni–P–CNTs in terms of surface morphology, mechanical and electrical characterizations, and device performance. Because the electroless-deposition technique is a cost-effective CMOS-compatible process, which can produce thick nanocomposite films in a low-processing-temperature environment ($<100°C$), the comparison is believed to provide an alternative process choice in the development of N/MEMS.

Material Synthesis and Device Fabrication

Electroless Ni-based nanocomposite plating solution preparation.— As the electroless deposition technique is applied to synthesize metal-based nanocomposites, how to make a colloidal plating solution is critical to the success of the process. Solutions with well-dispersed second-phase particles could ensure the particles uniformly engulfed into a metal matrix during the processing. Thus, in the preparation of 1 L Ni–P–diamond plating bath, a commercial Ni plating bath[3] composed of 150 mL Sheng-Hung chemical-nickel-plating (SCNP) A solution and 150 mL SCNP B solution is first mixed with a prewetted diamond powder (average size <500 nm) solution. Then, deionized (DI) water and ammonium hydroxide (NH_4OH) are utilized to modify the final pH value of the solution to 4.6 and make the solution volume 1 L. Finally, the plating solution, with good stirring, can be kept in pseudocolloid state for uniform deposition of Ni–P–diamond nanocomposite. The solutions with different diamond concentrations are premeditated to characterize fabrication process and material property, which are 0, 0.5, 1.0, and 2.0 g of the nanodiamond powders per liter of plating solution, respectively.

Multiwalled CNTs[4] (o.d.: 10–20 nm, i.d.: 5–10 nm, length: 0.5–200 μm, and bulk density: 0.04–0.05 g/cm^3) are chosen here for the synthesis of Ni–P–CNT nanocomposites. Because of the nonpolarized surface characteristic and fiber shape of CNTs, the CNTs curl and aggregate in water-based solutions, which cannot be separated using ultrasonication. The aggregation results in the occurrence of nonuniformity in the synthesized nanocomposite film. Therefore, an acidic oxidative method[5] is utilized to modify the surface chemistry of the CNTs that makes the nanotubes well dispersed in water. The following is the preparation of the Ni–P–CNT plating solution: The CNTs are first added into an acidic solution of 30 mL H_2SO_4 and 20 mL H_2O_2 mixture. After that, the acidic solution is sonicated for 30 min to keep the CNTs uniformly separate and form a colloidal solution with a negative pH value. Via the treatment, carboxylate COO^- groups are formed on the sites of the defects and the imperfect ends of the tubes. It can effectively avoid the self-curl phenomenon and the aggregation between the tubes.

After the treatment, the acidic CNT solution is distilled at 250°C for 30 min to fully decompose the residual H_2O_2 into H_2O and O_2 and subsequently mixed with the aforementioned commercial Ni–P plating solution. Finally, for the neutralization of the Ni–P–CNT plating solution, DI water and NH_4OH are utilized to make the solution with a pH value of 4.6 and a total volume of 1 L. The decomposition procedure is critical to the following plating process

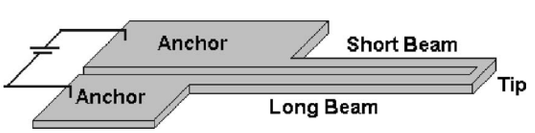

Figure 1. The schematic diagram of the long-short-beam electrothermal microactuator.

[z] E-mail: ytcheng@mail.nctu.edu.tw

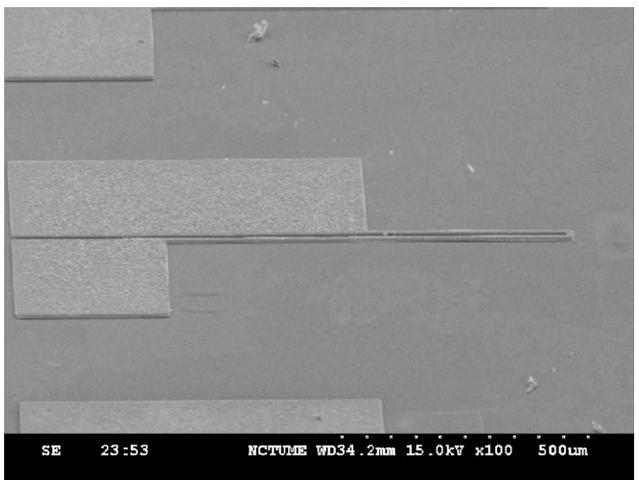

Figure 2. SEM micrograph of the fabricated Ni-P-diamond electrothermal microactuator.

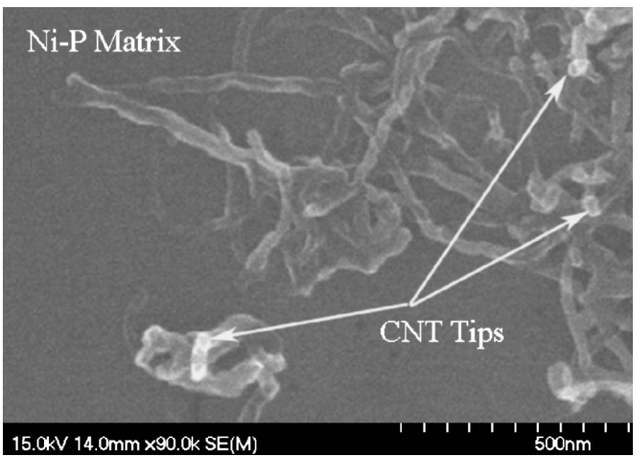

Figure 4. Highly magnified SEM micrograph of the Ni–P–CNT nanocomposite film in which some CNTs have one end buried inside the matrix as a root and the other end pointing outward as a tip.

because the mixture of NH_4OH and the residual H_2O_2 in the acidic CNT solution will chemically react with Cu and result in the disappearance of the seed layer on the wafer. Similarly, four different kinds of Ni–P–CNT plating baths containing 0, 0.007, 0.014, and 0.028 g/L of plating solution, respectively, are also prepared for characterization and comparison.

Design and fabrication of electrothermal microactuator.— The electrothermal microactuator is based on the long-short beam design[6] as shown in Fig. 1, which consists of a pair of connected adjacent cantilever beams with different lengths. By resistively heating these two beams, unequal thermal expansions make the joint of the beams toward the shorter one and provide a lateral actuation. In the design, the length ratio of the long beam to the short one is 2 and the length of the longer beam is 800 μm. Both beams are 10 μm wide and 9 μm thick. The gap between these two beams is 10 μm. The fabrication of the microactuator starts with a 2-μm high-density plasma, chemical vapor deposited (HDP-CVD) SiO_2 deposition as the electrical insulation and sacrificial layer. A seed layer of Ti/Cu (100 Å/500 Å) is then sputtered on top of the SiO_2, followed by a 10-μm thick AZP-4620 photoresist (PR) deposition. The PR is patterned and utilized as the device mold. Prior to the plating process, the wafer is dipped into a Pd seeding solution for 30 min to activate the copper surface. Pd ions chemically catalyze the redox reaction once the seeded wafer is immersed in the plating bath. After being seeded, the wafer is put into the colloidal plating bath for a 9-μm-thick nanocomposite film deposition in which the temperature is kept at 78°C. The whole process takes a total of 90 min for both cases. When the plating process is done, acetone and the mixture of NH_4OH and H_2O_2 solution are utilized to remove the PR mold and

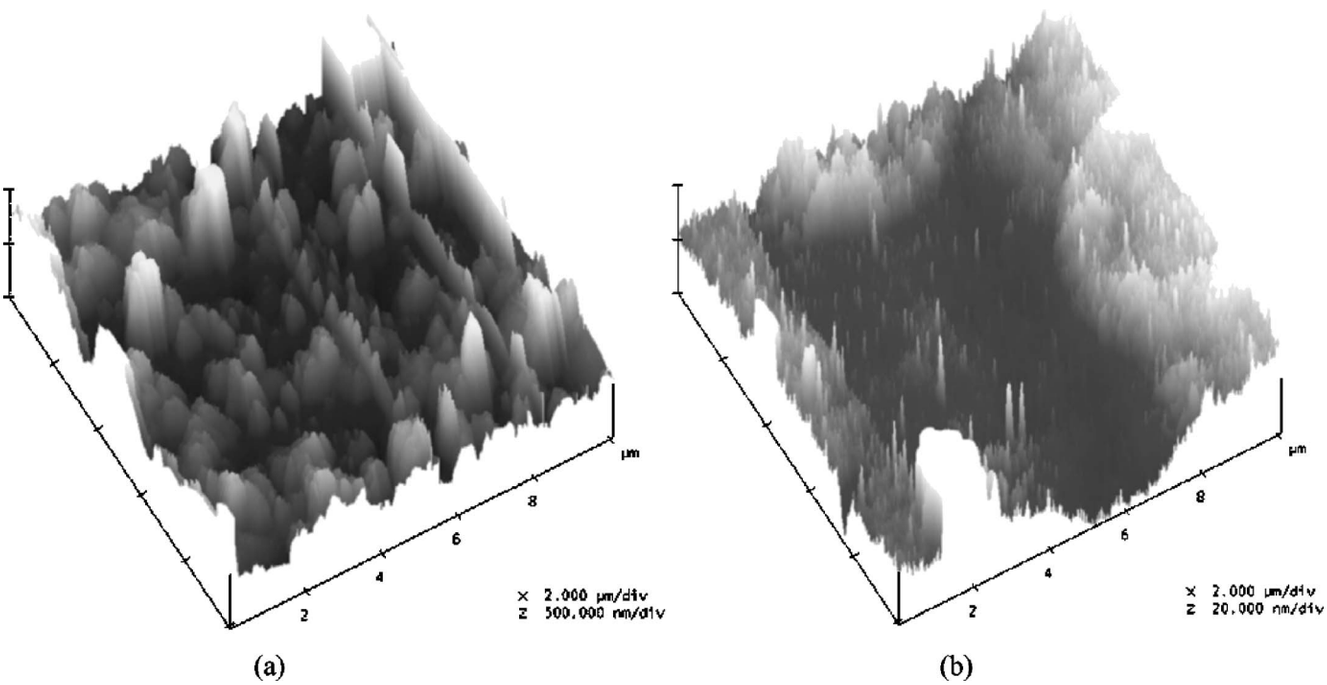

Figure 3. The surface morphology of the AFM image for the (a) Ni–P–diamond nanocomposite film and (b) Ni–P–CNT nanocomposite film.

Table I. The measured weight fractions and volume fractions of the two composites with different plating bath concentrations.

	Pure Ni (%)	CNTs: 0.007 g/L (%)	CNTs: 0.014 g/L (%)	CNTs: 0.028 g/L (%)	D: 0.5 g/L (%)	D: 1.0 g/L (%)	D: 2.0 g/L (%)
Weight fraction	0	0.075	0.11	0.215	1.575	1.84	2.715
Volume fraction	0	11.79	16.4	28.2	4.061	4.757	7.083

the copper seed layer, respectively. Finally, the electrothermal microactuator is fabricated after the removal of the Ti and SiO_2 sacrificial layer using hydrofluoric acid. Figure 2 shows the scanning electron microscopy (SEM) photograph of the electrothermal microactuators made of the Ni–P–diamond nanocomposite material.

Results and Discussion

Surface morphology and composition analysis.— Atomic force microscopy (AFM) is utilized to observe the surface morphology and roughness of the nanocomposite films. The average roughness of the Ni–P–diamonds is about 137.66 nm. The value is ten times larger than that of Ni–P and Ni–P–CNT films, which are about 12.628 and 8.996 nm, respectively. In addition, the morphologies of the two nanocomposites are quite different, as shown in Fig. 3. In comparison with the granular shape on the surface of the Ni–P–diamond film (see Fig. 3a), an acicular appearance exists on the Ni–P–CNT film surface (see Fig. 3b). These differences could be attributed to the size and inherent structures of the diamond powders and the CNTs. A highly magnified SEM image can further verify this point. As shown in Fig. 4, CNTs are dispersed on the Ni–P matrix to form the Ni-P-CNT nanocomposite film. Some CNTs have one end buried inside the matrix as a root and the other end pointing outward as a tip, which results in the acicular appearance. Because the o.d. of the CNT is only about 10 nm, which is smaller than the size of nanodiamond (~500 nm in diameter), the surface of Ni–P–diamond nanocomposite film should be much rougher than that of Ni–P–CNT film.

Energy-dispersive spectroscopy (EDS) is then utilized for the verification of the second phase incorporation. As shown in Fig. 5, the carbon peaks indicate the real existence of the diamond powders and CNTs embedded in the Ni–P matrix, respectively. Meanwhile, the plating process is characterized via the analysis of an elemental analyzer (EA). With the EA analyses, the weight fractions of CNTs or diamond powders in the Ni matrices with different plating concentrations are measured and listed in Table I. The volume fractions of CNTs and diamond powders in the matrices are calculated based on the density of nickel (8.908 g/cm^3), the density of diamond powder (3.51 g/cm^3), and the bulk density of multiwalled CNT (0.05 g/cm^3). The analyses show that the concentration of the embedded CNTs or diamond powders increases with the amount of CNTs or diamond powders which were added into the plating bath.

Nanoindentation tests.— The mechanical properties of nanocomposite films are first characterized using nanoindentor from which the hardness and Young's modulus of thin film can be measured.[7] Figure 5 shows the measurement results. The Young's modulus and hardnesses of the Ni–P–CNT nanocomposites plated with aforementioned different CNT concentrations are 165.1 ± 2.2, 180 ± 1.9, 187.2 ± 5.3, and 665.9 ± 20.6 GPa, respectively, as shown in Fig. 6a. The corresponding hardness values are 6.7 ± 0.1, 7.3 ± 0.1, 8.7 ± 0.4, and 28.9 ± 1.4 GPa. These results show the existence of mechanical strengthening effect in the Ni–P–CNT nanocomposite films. According to the EA measurement results, both the Young's modulus and hardness increase with the amount of CNT incorporation. However, in comparison with the one plated in the 0.028 g/L CNT solution, the composite films, plated in 0.007 and 0.014 g/L CNT bath, respectively, only have slightly larger Young's modulus and hardness than that of the pure nickel film. It is conjectured that the Young's modulus and hardness of a nickel matrix film can be dramatically enhanced while the concentration of the CNTs embedded in the Ni matrix exceeds a threshold value. Although similar mechanical property enhancements such as hardness and wear resistance increase in Ni–P–CNT nanocomposites have been reported,[8-10] none of them investigated the concentration dependence of the enhancements and found the anomalous phenomenon. Thus, further characterization is required for the understanding of possible causes.

In contrast, the nanoindentation testing results of the Ni–P–diamond films are different to that of Ni–P–CNT films. The Young's modulus and hardness of the Ni–P–diamond films decrease with

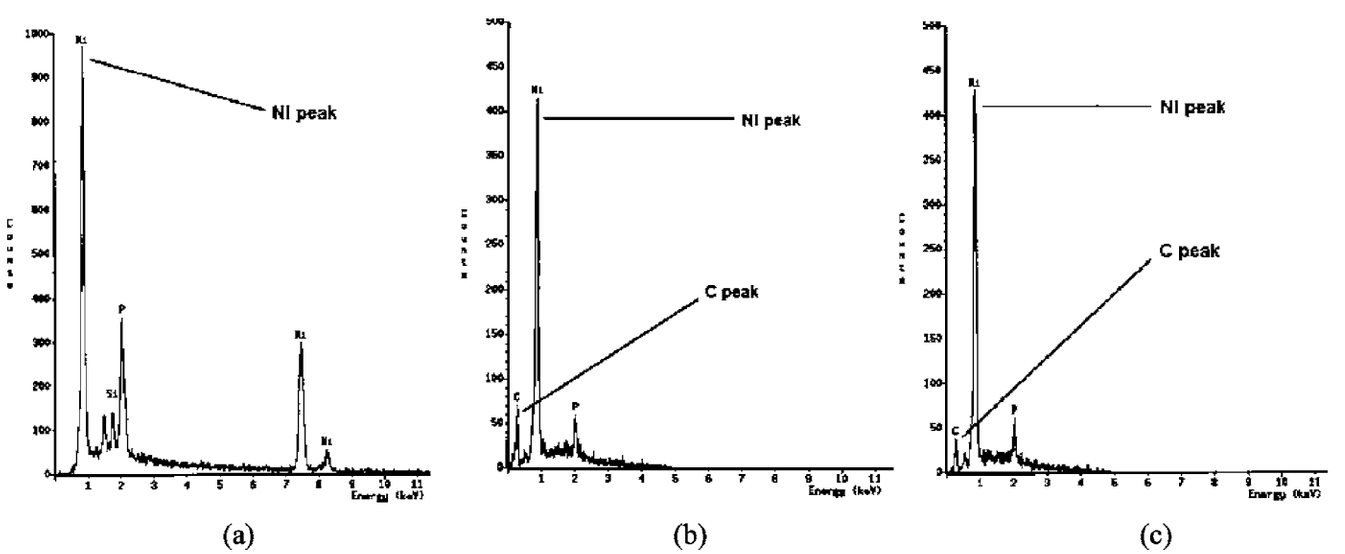

Figure 5. The EDS spectrums of the pure Ni–P film (a), the Ni–P–CNT (b), and the Ni–P–diamond (c) nanocomposite film.

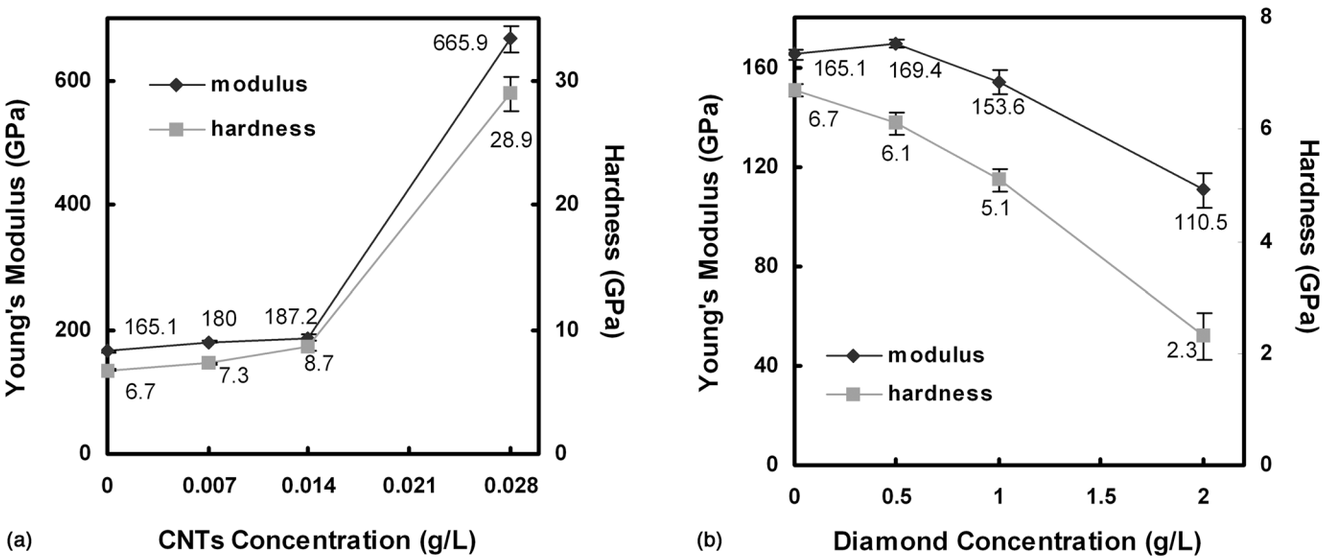

Figure 6. The nanoindentation test results of the four films with different (a) CNTs and (b) diamond concentrations.

the increase of the diamond concentration in the plating bath, as shown in Fig. 6b. In comparison with the Young's modulus and hardness of the pure Ni–P film, which are 165.1 ± 2.2 and 6.7 ± 0.1 GPa, the Ni–P–diamond films plated in the bath with 2.0 g/L diamond powders have much lower values, which are 110.5 ± 4.3 and 2.3 ± 0.1 GPa. The mechanical property degradation can be attributed to the crack formation on the surface of the nanocomposites. Figure 6 shows both SEM photographs of the Ni–P–diamond and Ni–P–CNT nanocomposite films. The surface appearances are different. Cracks and voids were found on the surface of the Ni–P–diamond nanocomposite film, as shown in Fig. 7a. On the contrary, the Ni–P–CNT composite film has smooth morphology and no observable surface defects as shown in Fig. 7b. According to the previous investigations, pores and cracks will result in the decrease of the Young's modulus and hardness measured by the nanoindentation.[11,12]

Young's modulus-to-density (E/ρ, $Pa\ m^3/kg$) ratio analysis.— In general, the E/ρ ratio is an important factor in the design of high-frequency, resonant MEMS. High E/ρ ratio represents a structural material with high rigidity but low density. Utilizing a material with a high E/ρ ratio for resonant MEMS fabrication can provide flexibility in device design. For instance, a cantilever-beam-type resonator, either with a thicker but shorter structure or with a higher E/ρ ratio structural material, can have a higher resonant frequency. However, the high E/ρ ratio can ease problems resulting from the limits of manufacturing cost and lithography in N/MEMS fabrication. In the experiment, cantilever beams are fabricated to characterize the E/ρ ratios of the Ni–P–CNT and Ni–P–diamond nanocomposite films. The fabrication process of the cantilever beams is similar to that of electrothermal actuators except for the bottom silicon substrate removal using tetra-methyl-ammonium hydroxide (TMAH)

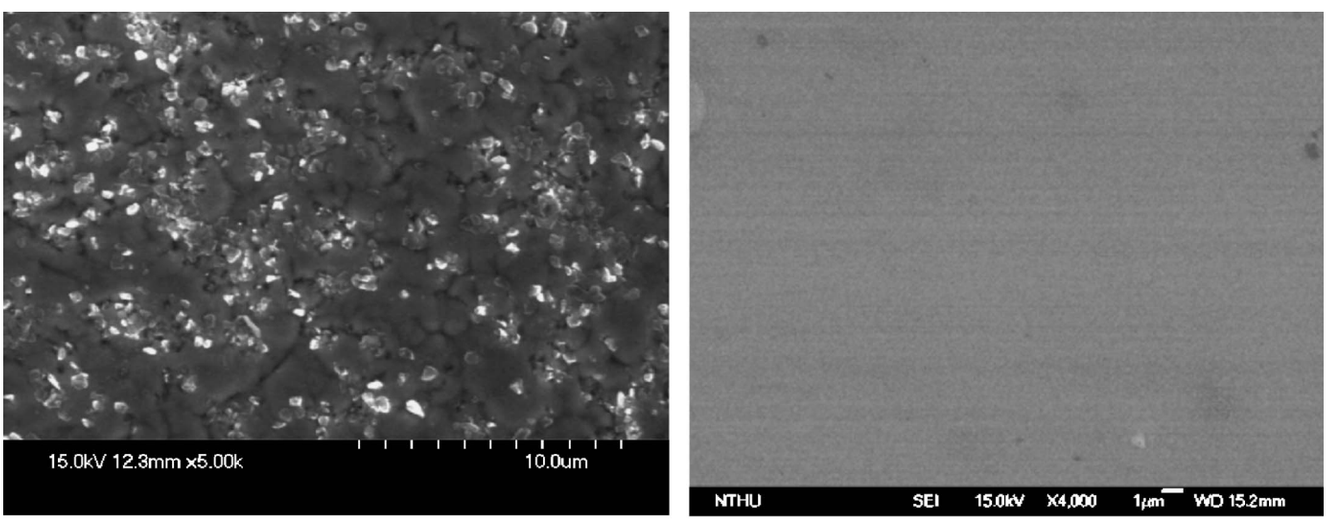

Figure 7. The SEM photo of (a) Ni–P–diamond film surface that contains some cracks and voids and (b) Ni–P–CNT film surface.

Table II. The measured resonant frequency and dimension of the selected cantilever beam.

	Beam width (μm)	Beam length (μm)	Beam thickness (μm)	Resonant frequency (kHz)
Pure Ni	50	352	8.6	24.013
CNTs: 0.007 g/L	50	358	8	24.08
CNTs: 0.014 g/L	51	358	7	32.298
CNTs: 0.028 g/L	50	358.7	7.3	38.567
D: 1.0 g/L	50	352	7.2	32.891
D: 2.0 g/L	51	351	5.3	25.409

etchant for vertical resonant frequency measurement.[13] A laser doppler vibrometer (LDV) is utilized here to measure the resonant frequency of the cantilever beam. Table II lists the measured frequencies together with the dimensions of the corresponding cantilever beams. According to the results, the E/ρ ratios of the nanocomposites can be extracted based on the following equation[14]

$$f = 0.1615\frac{h}{L^2}\sqrt{E/\rho} \qquad [1]$$

where h,L,E, and ρ represent the thickness and length of the cantilever beam and the Young's modulus and density of the device's material, respectively. The derived E/ρ ratio of the Ni–P–CNT nanocomposite film plated in the bath with 0.028 g/L CNT is 3.8 times larger than that of the pure Ni–P, as shown in Fig. 8. Similarly, the E/ρ ratio of the Ni–P–diamond film has also about 3 times augmentation. Because the resonant frequency or the ratio increases with the concentration of the embedded second phase, the tendency indicates that both kinds of nanocomposite materials have potential for the production of high-frequency MEMS microresonators in comparison with pure Ni.

In addition to the dynamic measurement of the E/ρ ratio, the E/ρ ratio can be also derived by directly dividing the Young's modulus by the effective density which is obtained by the previous nanoindentation test and the rule of mixtures (ROM),[15,16] respectively. According to the ROM, the effective density (ρ_{eff}) of the composite is estimated as the following

$$\rho_{\text{eff}} = \rho_c f_c + \rho_m f_m \qquad [2]$$

where ρ_c,f_c,ρ_m, and f_m are the densities and volume fractions of the embedded second phase and the matrix material, respectively. The E/ρ ratios derived from the calculation are shown in Fig. 8 and compared to that from the previous resonant frequency measurement results. It is found that the calculated E/ρ ratios are larger in both Ni–P–CNT and Ni–P–diamond composite films. The difference between the two derivations is mainly caused by the undercut effect of the cantilever anchor pad.[17] The pad area with the undercut effect also takes part in the vibration of the cantilever beam and results in the effective length increase of the cantilever beam and the reduction of the resonant frequency. Without considering the undercut effect, the dynamic E/ρ ratios will be underestimated. Moreover, in the case of the Ni–P–diamond composites, it is found that the calculated ratios decrease with the increase of the embedded diamond concentration as previously mentioned. The tendency could be attributed to the decrease of Young's modulus and the overestimation of ρ_{eff} due to the existence of cracks and voids. The calculation of ρ_{eff} is made based on the assumption of the perfect composite structure where no structural defects exist. In fact, it also explains why the distinct tendency does not appear in the case of the Ni–P–CNT films because no surface defects have been found.

Electrical property analyses.— For electrical characterization, four-point probe measurement is utilized to measure the sheet resistance of the nanocomposite films. The intrinsic bulk resistivity of Ni–P–CNT or Ni–P–diamond composite film is obtained by multiplying the sheet resistance by film thickness. Figure 8 shows the resistivities of the Ni–P–diamond and the Ni–P–CNTs vs the concentrations of the diamond powders and CNTs in the plating baths, respectively. Both resistivities increase with the incorporated concentration of the embedded diamond powders and CNTs. For the Ni–P–diamond composite films, the diamond powder is an insulator that contributes no electrical conductivity to the Ni matrix. In contrast, the embedded multiwalled CNT is electrically conductive along the longitudinal direction. Based on the model of two-phase random network, the Maxwell-Wagner equation described in Eq. 3 is utilized for the characterization of the electrical conductivity of the composites.[18] The conductivity of Ni–P–diamond nanocomposite film can be approximated in Eq. 4 with $k_m \gg k_d$

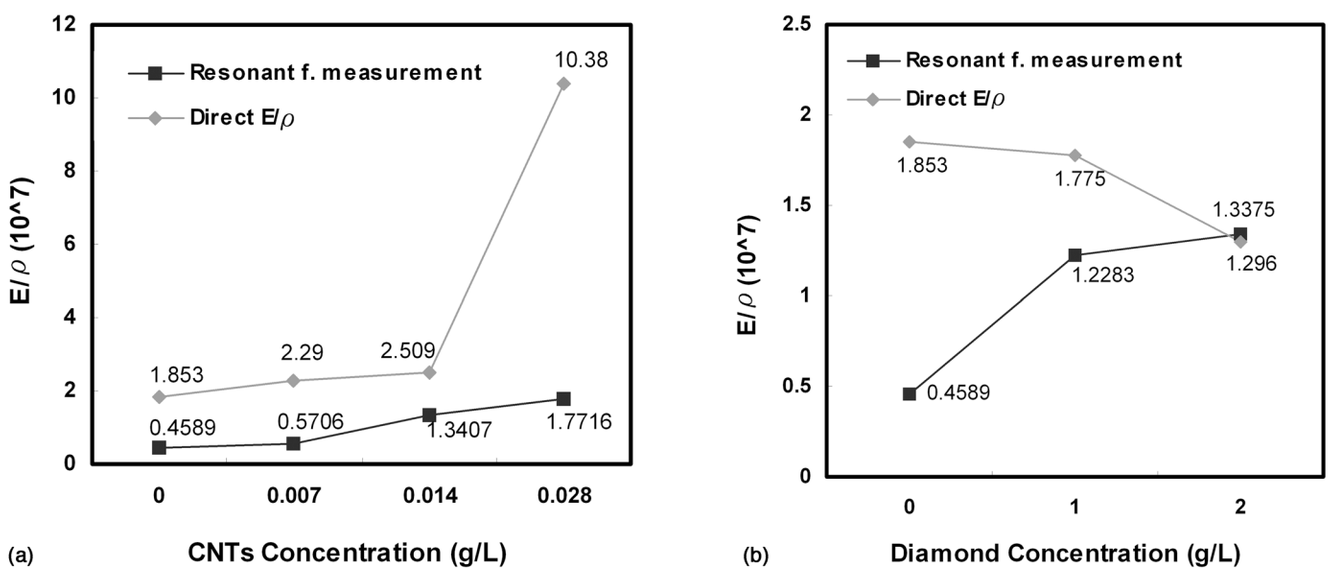

Figure 8. The obtained E/ρ ratio diagram of the (a) Ni–P–CNT films and (b) Ni–P–diamond film.

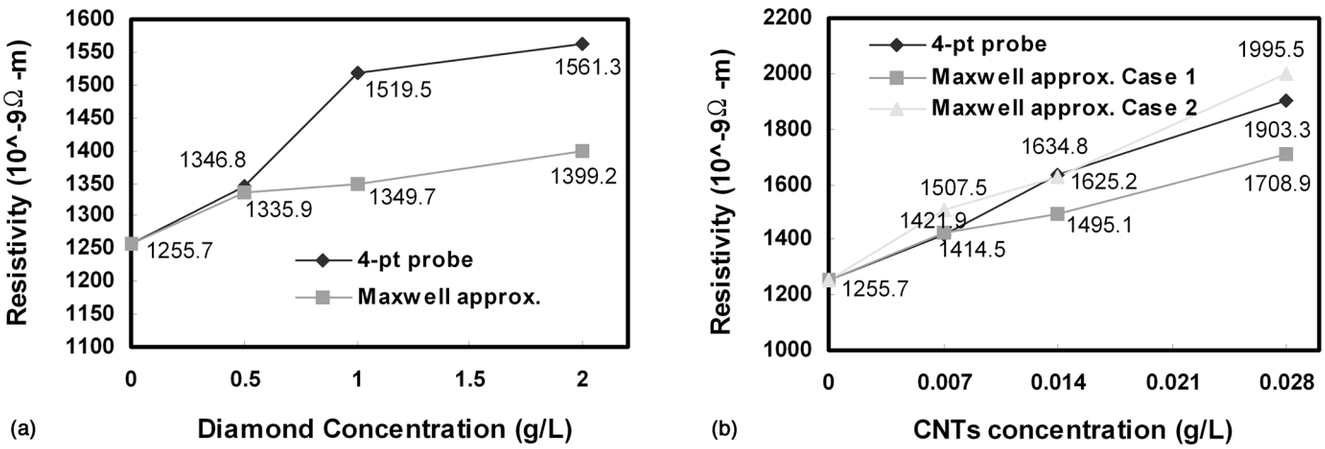

Figure 9. The diagram of sheet resistances measured by four-point probe and theoretical calculations using Maxwell-Wagner two-phase model for different concentrations of (a) CNT and (b) nanodiamond nanocomposite films in the plating solutions.

$$k_c = k_m \frac{1 + 2V_f(1 - k_m/k_d)/(1 + 2k_m/k_d)}{1 - V_f(1 - k_m/k_d)/(1 + 2k_m/k_d)} \quad [3]$$

$$k_c = k_m(1 - V_f)/(1 + V_f/2) \quad [4]$$

where k_c,k_m, and k_d are the electrical conductivities of the composite film, the Ni matrix, and the second phase, respectively, and V_f is the volume fraction of the second phase listed in Table I. The results are plotted in Fig. 9 by substituting the known parameters k_m and V_f into Eq. 4. The resistivity measured with four-point probe in 0.5 g/L diamond concentration is matched with the theoretical calculation using the Maxwell-Wagner equation as shown in Fig. 9a. However, large discrepancy between the measurement results and theoretical predictions occurs in the films plated with 1.0 and 2.0 g/L diamond concentrations. The discrepancy might result from the increase of cracks and voids. For the case of Ni–P–CNTs as shown in Fig. 9b, because CNT is a tube-shaped structure with the electrical conductivity along the longitudinal direction, two extreme cases (parallel or perpendicular to the current flow direction) are applied on the Maxwell-Wagner model to check the relations between the electrical resistivity and embedded CNT volume fractions in the composite. For the extreme case of the embedded CNTs oriented along the current flow direction, the conductivity of the CNTs should be considered and the total conductivity of the composite film is the same as the two-phase Maxwell-Wagner equation. In the second extreme case, the orientation of the embedded CNTs is perpendicular to the direction of current flow and the CNTs will contribute nil conductivity to the composite film, i.e., $k_m \gg k_d$. Thus, the conductivity of the Ni–P–CNTs can also be simplified as Eq. 4. Figure 9 shows that the resistivity of the Ni–P–CNT films increases with the concentration of the embedded CNTs in the nanocomposite film due to the higher resisitivty of CNTs (5.4×10^{-4} Ω cm) in comparison with that of pure nickel (1.26×10^{-4} Ω cm). As compared, the resistivities of the Ni–P–CNT composites obtained by four-point probe measurement fall just within two extreme cases, indicating that the distribution of CNTs in the film is in a random dispersion that is all neither parallel nor perpendicular to the direction of the current flow. The electrical characteristics can be estimated with upper and lower bonds.

Displacement measurements of the electrothermal microactuator.— Figure 10 shows the measurement results of the electrothermal microactuators made of the pure Ni–P, the Ni–P–CNT nanocomposite plated in the bath with 0.028 g/L CNTs, and the Ni–P–diamond nanocomposite plated in the bath with 1.0 g/L diamond powders, respectively. The data of the input power vs displacement reveals that the performance of the microactuator made of the Ni–P–CNTs has been greatly improved in terms of the displacement and power efficiency of the device in comparison with that made of pure Ni–P film. The maximum displacement of the Ni–P–CNT actuators is about 10 μm, which is four times larger than that of the pure one only with 2.5-μm displacement. Meanwhile, for a 2-μm displacement, the input power of the Ni–P actuator is about 0.12 W, which is 5 times larger than that of Ni–P–CNTs (0.024). The result shows excellent power efficiency using the Ni–P–CNTs as the structural material for the electrothermal microactuator fabrication.

The maximum displacement of the actuators made of Ni–P–diamond can also reach 10 μm, which is similar to the Ni–P–CNTs. With the same displacement of 2 μm, the input power of the Ni–P actuator is about 6 times larger than that of the device made of the Ni–P–diamond nanocomposite (0.02 W). The electrothermal actuator enhancement is similar to our previous report in the system of electrolytic Ni/diamond nanocomposites,[19] even with more power efficiency and larger displacements. However, for the microactuator made of the Ni–P–diamond, there is a displacement plateau at the

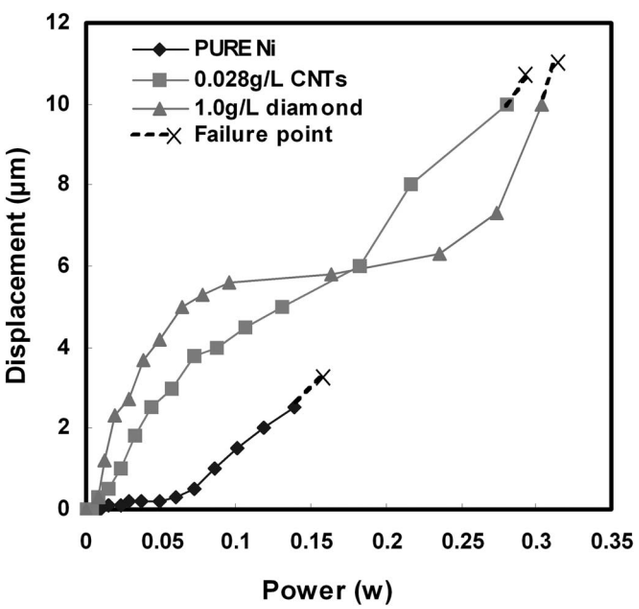

Figure 10. The diagram of power vs displacement for pure Ni, Ni–P–CNT, and Ni–P–diamond electrothermal microactuators.

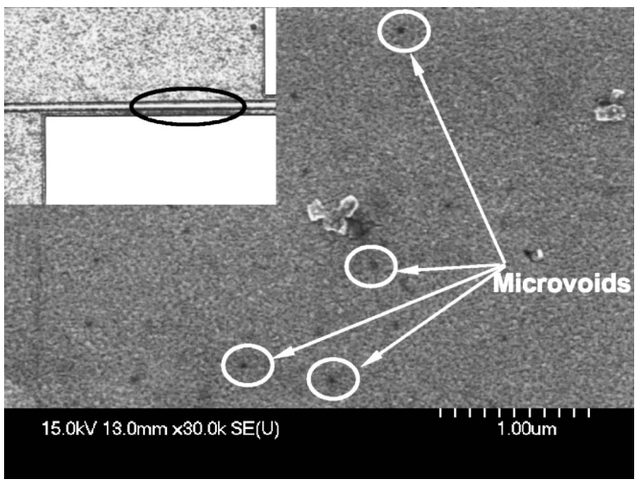

Figure 11. SEM photo of Ni–P–diamond electrothermal actuator dark region surface after applied power to 0.26 W.

input power range from 0.1 to 0.3 W. Such a phenomenon can be attributed to the formation of many microvoids which are further validated by the surface micrograph of the Ni–P–diamond electrothermal actuator after being applied 0.26-W power input, as shown in Fig. 11. The picture is taken in the hottest region of the actuator in which microvoids are formed on the surface while the power input falls in the region of the plateau. In addition, Fig. 11 shows that no cracks exist on the surface in comparison with Fig. 7a, though the device structure is plated in the bath with 1.0 g/L diamond nanopowders. The inconsistence could be caused by the slender geometry of that actuator arm, which makes less diamond incorporation than that of the contact pad during the plating process. More investigations are required to verify the hypothesis.

Conclusion

The Ni–P–diamond nanocomposite films and related MEMS devices were successfully synthesized, fabricated, and compared with that of Ni–P–CNTs in terms of mechanical and electrical properties and device performance, respectively. In comparison with pure Ni, the incorporation of nanodiamond powders into the electroless Ni matrix can enhance the E/ρ ratio of the Ni–P–diamond nanocomposite film with three times increase while the film is plated in a bath with 2.0 g/L nanodiamond powders. That is similar to the case of Ni–P–CNTs in which about four times increase can be realized while the film is synthesized in the bath with 0.028 g/L CNTs. The enhancements make these films fascinating for high-frequency resonating device fabrications. ROM and the Maxwell-Wagner equation can appropriately illustrate the electrical properties of the nanocomposites by introducing an upper and a lower bond estimate. In addition, the actuators made of both the nanocomposites can provide 10-μm displacement that is 4 times larger than that made of pure Ni. Although voids and cracks have been found in the Ni–P–diamond nanocomposite that could result in reliability problems and require further process development to prevent defect formation, both Ni–P–diamond and Ni–P–CNT nanocomposites have shown the potential application for MEMS fabrication due to their superior compatibility with contemporary CMOS manufacturing processes.

Acknowledgment

The authors thank the Nano Facility Center of National Chiao Tung University, Professor Fang at National Tsing Hua University, and Professor Lin at Hwa Hsia College of Technology and Commerce for providing technical support and measurement facilities. This work was supported by the NSC 93-2220-E-009-002 project and in part by the MediaTek Research Center at National Chiao Tung University.

National Chiao Tung University assisted in meeting the publication costs of this article.

References

1. K. S. Teh, Y. T. Cheng, and C. Sambucetti, in *IEEE Micro Electro Mechanical Systems Conference*, Las Vegas, NV, p. 384 (2002).
2. G. R. Shen, L. N. Tsai, Y. T. Cheng, W. Hsu, and T. K. Lin, *IEEE Conference on Nanotechnology*, München, Germany, p. 192, (2004).
3. Sheng Hung Chemical Engineering Co., Ltd., http://www.shccl.com.tw
4. Seedchem Company PTY, Ltd., Camberwell 3124 Vic Melbourne, Australia.
5. W. Zhao, C. Song, and P. E. Pehrsson, *J. Am. Chem. Soc.*, **124**, 12418 (2002).
6. K. Lu and M. L. Sui, *Acta Metall. Mater.*, **43**, 3325 (1995).
7. L. Riester, P. J. Blau, E. Lara-Curzio, and K. Breder, *Thin Solid Films*, **377**, 635 (2000).
8. W. X. Chen, J. P. Tu, L. Y. Wang, H. Y. Gan, Z. D. Xu, and X. B. Zhang, *Carbon*, **41**, 215 (2003).
9. Y. L. Shi, Z. Yang, H. Xu, M. K. Li, and H. L. Li, *J. Mater. Sci.*, **39**, 5809 (2004).
10. J. N. Balaraju, T. S. N. Sankara Narayanan, and S. K. Seshadri, *J. Appl. Electrochem.*, **33**, 807 (2003).
11. Z. H. Xu and D. Rowcliffe, *Surf. Coat. Technol.*, **161**, 44 (2002).
12. G. E. Fougere, L. Riester, M. Ferber, J. R. Weertman, and R. W. Siegel, *Mater. Sci. Eng., A*, **204**, 1 (1995).
13. H. C. Tasi and W. Fang, *Sens. Actuators, A*, **103**, 377 (2003).
14. S. Timoshenko, D. H. Young, and W. Weaver, Jr., *Vibration Problems in Engineering*, 4th ed, John Wiley & Sons, New York (1974).
15. W. D. Callister, Jr., *Materials Science and Engineering*, 3rd ed., p. 516, John Wiley & Sons, New York (1994).
16. G. E. Dieter, *Mechanical Metallurgy*, 3rd ed., Chap. 6, pp. 184–240, McGraw-Hill Book Company, New York (1978).
17. H. C. Tsai, J. M. L. Tsai, H.-C. Chang, and W. Fang, in *The 12th International Conference on Solid State Sensors, Actuators and Microsystems, Transducers'03*, Boston, MA, p. 482 (2003).
18. D. G. Han and G. M. Choi, *Solid State Ionics*, **106**, 71 (1998).
19. L. N. Tsai, G. R. Shen, Y. T. Cheng, and W. Hsu, in *IEEE ECTC*, Las Vegas, NV, p. 472 (2004).